Charged rodlike colloidal suspensions: An ab initio approach

Hartmut Löwen

Articles you may be interested in

Charged rodlike colloidal suspensions: An *ab initio* approach

Hartmut Löwen
Sektion Physik der Universität München, Theresienstrasse 37, D-80333 München, Germany

The interactions and orientational correlations of charged rodlike colloidal particles in a salt-free suspension are calculated using an "*ab initio*" approach which combines molecular dynamics for the rods and classical density functional theory for the counterions. Both fluid and liquid-crystalline phases are investigated. It is found that the interaction between charged rods can satisfactorily be described by an effective Yukawa-segment model which in general differs, however, from the Derjaguin–Landau–Verwey–Overbeek segment model. For strongly interacting long rods, an exactly soluble Yukawa-segment model, based on a cylindrical Poisson–Boltzmann cell, is proposed which reproduces the *ab initio* data quite well in the liquid-crystalline phase.

I. INTRODUCTION

Highly charged colloidal suspensions of rigid rodlike particles represent excellent realizations of liquid-crystalline systems.[1-3] Well-known examples are concentrated aqueous suspensions of tobacco–mosaic viruses (TMV) or bacterial *fd* and *Pf*1 viruses,[4] but there are also other realizations like cylindrical micellar aggregates (see, e.g., Refs. 5 and 6), colloidal β-FeOOH,[7] γ-AlOOH,[8] polytetrafluoroethylene,[9] and ellipsoidal polystyrene latex particles.[10] Suspensions of such rodlike particles reveal a number of new phases and also show characteristic structural and dynamical effects typical for liquid crystals which are not observed in suspensions of spherical particles. Since the first experimental proof of the existence of liquid-crystalline order in a TMV suspension by Bawden *et al.* in 1936[11] there has been a flurry of detailed experimental investigations for the TMV and *fd* viruses and related systems. The experimental studies make use of static and dynamical light scattering as well as small angle neutron scattering (as for recent experiments see Refs. 12–20 and for a review on earlier experiments see, e.g., Ref. 21). These studies have essentially contributed to our understanding of the structure and dynamics in the disordered phase and have also revealed a number of other liquid-crystalline phases, like nematic, smectic A, smectic B, and columnar phases. Despite these numerous investigations, the complete phase diagram for a given material (as TMV) is still not entirely understood over the full range of densities, temperature, and for different charges on the cylindrical rods, and one can be optimistic that new liquid-crystalline phases may still be discovered in rodlike suspensions.

Theoretically, one mainly has tried to capture the essential physics within a simple model of hard ellipsoids or hard spherocylinders. This idea originates from Onsager[22] and was also used to interpret experimental data qualitatively.[23,13] By Monte Carlo simulation, the phase diagram was calculated[24] for different length to width ratios of the rods, showing disordered, nematic, and smectic phases. This phase diagram was also obtained by current density functional theories.[25-28] It is clear that a model of hard rodlike particles is greatly oversimplified for a quantitative description of the real interaction of charged rods where the long-ranged Coulomb interaction between the rods and their counterions is dominant. The Coulombic repulsion between the rods is screened by a counterion cloud around the cylindrical rods. If one adds salt to the solution, screening is drastically enhanced by the additional salt ions. It is only in the extreme strong screening limit (i.e., for a high concentration of added salt) that a hard-body model is justified. Particularly, for typical experimental parameters, where one often works in the salt-free limit, a hard-body model must fail.

A more realistic attempt for the interaction between charged rods was done by Klein and co-workers.[29-31] At infinite solution, they have shown that a Derjaguin–Landau–Verwey–Overbeek (DLVO)–Yukawa-segment model, to be described later, is an adequate description of the interaction.[32] In this model, the interaction is described in terms of an effective pair potential between the rods. Klein *et al.* then assumed that the DLVO-segment model is valid also for higher concentrations and calculated structural correlation using liquid integral equations and Monte Carlo simulations.[33] However, one should note that the validity of the DLVO model is an *ad hoc* assumption which may give qualitative agreement with experiments but still needs to be justified theoretically.

The most general framework for a theoretical description of the structural correlations and the interaction between rodlike polyelectrolytes is constituted by the so-called "primitive" approach where the discrete structure of the solvent is neglected completely and the interaction between the rods and their counterions is a combination of Coulombic and excluded volume interactions. Due to the complete timescale separation between relaxations of microscopic counterions and mesoscopic rods, the adiabatic approximation is well justified. This implies that only the density field of the counterions is a relevant variable which adjusts itself adiabatically in the external field made up by the charged rods. This adiabatic primitive approach was frequently used to study the structure and dynamics for *spherical* colloidal particles. For instance the density profile in a spherical Wigner–Seitz cell around a single colloidal particle[34] was investigated. Recently, also an *ab initio* simulation[35-37] of the structural correlation of macroions was performed using a classical version of the Car–Parrinello algorithm.[38] In this approach, one could directly simulate the adiabatic primitive model and thus predict structural and dynamical properties.

For charged colloidal rods, however, much less theoretical work was done due to the enhanced complexity of the problem. The orientational degrees of freedom drastically increase the effort of solving a suitable closure relation of a liquid integral equation. There are, however, some simple situations which are understood better. The density profile around a single infinitely long rod was studied by liquid integral equations by Rossky and co-workers.[39,40] This quantity was also directly measured in a small-angle x-ray scattering experiment of Wu et al.[6] Although the counterion density distribution is a key quantity in understanding screening effects, the interaction between two rods and their static correlations are more complicated quantities which are not trivially connected to the density profile. Second, Dhont[41] studied the structure of fully aligned rods.

In this paper, we transfer the *ab initio* description within the primitive approach, which was successfully applied already to the case of spherical colloidal particles, to colloidal rods. We have performed *ab initio* simulations of the counterionic screening where nonlinear screening effects and effective counterion-induced many-body forces and torques are included. As an output, we obtain center-of-mass and orientational correlations between the rods. Based on this calculation, we propose an effective optimal pair potential between the rods which fits the *ab initio* data well. This effective pair potential is very close to an effective Yukawa-segment model, but differs in general from the DLVO-segment model. Thus the Yukawa-segment model of Klein *et al.* is justified if the effective charges and the screening parameter are suitably chosen. We propose an exactly solvable Poisson–Boltzmann cell model which works for strongly interacting rods and gives reasonable predictions for the effective charge and the screening parameter if the system is in a phase where the rods are at least partially aligned.

The paper is organized as follows: The primitive approach and details of the *ab initio* description are introduced in Sec. II. Then, in Sec. III, different effective Yukawa-segment models are proposed and discussed. In Sec. IV, the numerical implementation of the *ab initio* method is outlined and results are summarized in Sec. V. Finally, we conclude and summarize the results in Sec. VI.

II. *AB INITIO* APPROACH: GENERAL THEORY

In the primitive approach, we start from a two-component system consisting of charged colloidal rods of mesoscopic size (macroparticles) and microscopic counterions. In the following, we shall restrict ourselves to the salt-free case. The discrete nature of the solvent is neglected completely, it manifests itself merely by its dielectric constant ϵ screening the Coulomb interaction between rods and counterions. The rods are cylindrical with a characteristic cylindrical radius R and a total length L. They carry a total charge Ze, Z typically lying between 100 and 10 000, which is distributed over the rod volume ν_m (the index m stands for macroparticle or rod) according to a charge density $en_m(\mathbf{r},\boldsymbol{\Omega})$ if the center of mass of the rod is at origin. Here, $\boldsymbol{\Omega}$ is a unit vector determining the orientation of the rod. The normalization of $n_m(\mathbf{r},\boldsymbol{\Omega})$ is such that $\int d\mathbf{r}\, n_m(\mathbf{r},\boldsymbol{\Omega})=Z$. The actual value of the rod volume ν_m depends a bit on whether one takes spherocylinders or pure cylinders, in any case $\nu_m \approx \pi R^2 L$. More generally, the shape of the rod with its center of mass at the origin is specified by a function $\chi(\mathbf{r},\boldsymbol{\Omega})$ which is defined as

$$\chi(\mathbf{r},\boldsymbol{\Omega})=\begin{cases} 1 & \text{if } \mathbf{r} \text{ is inside the rod} \\ 0 & \text{if } \mathbf{r} \text{ is outside the rod} \end{cases} \tag{1}$$

such that $\nu_m=\int d\mathbf{r}\,\chi(\mathbf{r},\boldsymbol{\Omega})$.

In the primitive model, the interactions result from a combination of Coulombic and excluded volume forces. The direct interaction between rods is then given by the following potential:

$$V_{mm}(\mathbf{r},\boldsymbol{\Omega}_1,\boldsymbol{\Omega}_2)=\begin{cases} \infty & \text{if there is a } \mathbf{r}' \text{ such that } \chi(\mathbf{r}',\boldsymbol{\Omega}_1)\chi(\mathbf{r}'+\mathbf{r},\boldsymbol{\Omega}_2)=1 \\ A(\mathbf{r},\boldsymbol{\Omega}_1,\boldsymbol{\Omega}_2) & \text{else} \end{cases} \tag{2}$$

with

$$A(\mathbf{r},\boldsymbol{\Omega}_1,\boldsymbol{\Omega}_2)=\int d\mathbf{r}' \int d\mathbf{r}'' \frac{e^2 n_m(\mathbf{r}',\boldsymbol{\Omega}_1) n_m(\mathbf{r}+\mathbf{r}'',\boldsymbol{\Omega}_2)}{\epsilon|\mathbf{r}'-\mathbf{r}''|}$$
$$\times \chi(\mathbf{r}',\boldsymbol{\Omega}_1)\chi(\mathbf{r}+\mathbf{r}'',\boldsymbol{\Omega}_2), \tag{3}$$

where $\mathbf{r}$ is the difference between the two center-of-mass rod positions and $\boldsymbol{\Omega}_i$ ($i=1,2$) is the orientation of rod i. The counterions are assumed to be pointlike and carry a charge $-qe$. Hence, the potential between a counterion and a rod with orientation $\boldsymbol{\Omega}$ is

$$V_{mc}(\mathbf{r},\boldsymbol{\Omega})=\begin{cases} \infty & \text{if } \chi(\mathbf{r},\boldsymbol{\Omega})=1 \\ -qe^2\int d\mathbf{r}' \dfrac{n_m(\mathbf{r}',\boldsymbol{\Omega})}{\epsilon|\mathbf{r}-\mathbf{r}'|}\,\chi(\mathbf{r}',\boldsymbol{\Omega}) & \text{else} \end{cases}, \tag{4}$$

where now $\mathbf{r}$ is the difference between the center of mass of the rod and the counterion position. The index c is for counterions. Finally, the counterions are treated as a classical plasma with interaction

$$v_{cc}(r)=\frac{q^2 e^2}{\epsilon r}. \tag{5}$$

Strictly speaking, two different charge distributions $en_m(\mathbf{r},\boldsymbol{\Omega})$ with the same line charge density along the rod lead to different interaction. In view of Gauss theorem for a cylindrical symmetry, however, the differences should be small. In the following we shall therefore only consider the line charge density as the essential parameter to characterize the rod charge distribution.

We consider N_m rods and N_c counterions in a given volume ν. Global charge neutrality then requires that

$$ZN_m = qN_c . \tag{6}$$

The thermodynamic parameters are the rod density $\rho_m = N_m/\nu$ (the counterion density is then fixed to be $\rho_c = N_c/\nu = Z\rho_m/q$) and the temperature T. The rod density ρ_m is conveniently measured in terms of $c^* \equiv 1/L^3$.

Having written down the basic interactions, we further adopt the adiabatic approximation.[36] If $\{R_i\}$ and $\{\Omega_i\}$ are the center-of-mass positions and orientations of the rods ($1 \leq i \leq N_m$), the total Lagrangian of the adiabatic primitive model reads

$$\mathcal{L} = \sum_{i=1}^{N_m} \left(\frac{1}{2} M\dot{R}_i^2 + \frac{1}{2} \Theta\dot{\Omega}_i^2 - \lambda_i(\Omega_i^2 - 1) \right)$$

$$- \sum_{i,j=1;i<j}^{N_m} V_{mm}(R_i - R_j, \Omega_i, \Omega_j)$$

$$- \mathcal{F}([\rho_c(r)], \{R_i\}, \{\Omega_i\}), \tag{7}$$

where M and Θ are the mass and the moment of inertia of the rods and $\{\lambda_i\}$ is a set of Lagrange multipliers ensuring that $|\Omega_i| = 1$. The dot denotes a time derivative. Finally, the adiabaticity condition manifests itself by the fact that merely the counterionic density field $\rho_c(r)$ enters into the equations of motion. The density functional $\mathcal{F}$ depends parametrically on the rod positions and orientations and can be split into four different terms:[36]

$$\mathcal{F} = \mathcal{F}_{id} + \mathcal{F}_{ext} + \mathcal{F}_{cc} + \mathcal{F}_{corr}, \tag{8}$$

where

$$\mathcal{F}_{id} = k_B T \int d\mathbf{r}\, \rho_c(\mathbf{r})\{\ln[\Lambda_c^3 \rho_c(\mathbf{r})] - 1\}, \tag{9}$$

$$\mathcal{F}_{ext} = \int d\mathbf{r}\, \rho_c(\mathbf{r}) V_{ext}(\mathbf{r}, \{R_j\})$$

$$= \sum_{j=1}^{N_m} \int d\mathbf{r}\, \rho_c(\mathbf{r}) V_{mc}(\mathbf{r} - R_j, \Omega_j), \tag{10}$$

$$\mathcal{F}_{cc} = \frac{q^2 e^2}{2\epsilon} \int \int d\mathbf{r}\, d\mathbf{r}'\, \frac{\rho_c(\mathbf{r})\rho_c(\mathbf{r}')}{|\mathbf{r} - \mathbf{r}'|} . \tag{11}$$

In the "ideal" part (9), Λ_c is the de Broglie thermal wavelength of the counterions; $\mathcal{F}_{ext}$ describes the coupling of the counterions to the rods, while $\mathcal{F}_{cc}$ stems from the Coulomb interaction between counterions. The last term in Eq. (8) is the nontrivial counterion correlation term, for which we adopt the local density approximation (LDA)

$$\mathcal{F}_{corr} = k_B T \int d\mathbf{r}\, \rho_c(\mathbf{r}) \Psi_{OCP}^{exc}(T, \rho_c(\mathbf{r})). \tag{12}$$

In Eq. (12), Ψ_{OCP}^{exc} denotes the reduced excess free energy per ion, $F^{exc}/Nk_B T$, of a homogeneous fluid of point ions in neutralizing, uniform background, for which we use the Abe expansion:[42]

$$\Psi_{OCP}^{exc}(T, \rho_c) = -\frac{1}{3}\, \Gamma^{3/2} - \frac{c}{3}\, \Gamma^3 - \frac{1}{8}\, \Gamma^3(3\ln\Gamma - 1)$$

$$+ O(\Gamma^{9/2}), \tag{13}$$

where $\Gamma \equiv (4\pi\rho_c/3)^{1/3} q^2 e^2/\epsilon k_B T$, k_B denoting Boltzmann's constant, $c = \frac{9}{8}\ln 3 + \frac{3}{2}\gamma - 1 = 1.101\,762\,3\cdots$, and γ is Euler's constant. The only approximation that has been made is the LDA for $\mathcal{F}_{corr}$ which is justified for parameters typical for colloidal suspensions except perhaps in the immediate vicinity of the rod surface where the counterions pile up, due to the strong Coulomb attraction.

For each rod configuration, the equilibrium one particle counterion density $\rho_c^{(0)}(\mathbf{r}, \{R_i\}, \{\Omega_i\})$ is the solution to the variational problem:

$$\left. \frac{\delta\mathcal{F}}{\delta\rho_c} \right|_{\rho_c = \rho_c^{(0)}(\mathbf{r})} = 0 \tag{14}$$

subject to the constraint of global charge neutrality:

$$\int d\mathbf{r}\, \rho_c(\mathbf{r}) = N_c = \frac{Z}{q}\, N_m . \tag{15}$$

Once $\rho_c^{(0)}$ has been determined, the forces $\mathbf{F}_j^c$ on the center of mass and the torques $\mathbf{M}_j^c$ induced by the counterions acting on each rod may be calculated directly, according to

$$\mathbf{F}_j^c = -\nabla_{R_j} \mathcal{F}([\rho_c^{(0)}(\mathbf{r}, \{R_i\}, \{\Omega_i\})]\{R_i\}, \{\Omega_i\})$$

$$= -\int d\mathbf{r}\, \rho_c^{(0)}(\mathbf{r}, \{R_j\}, \{\Omega_i\})\nabla_{R_j} V_{mc}(\mathbf{r} - R_j, \Omega_j) \tag{16}$$

and

$$\mathbf{M}_j^c = -\Omega_j \times \nabla_{\Omega_j} \mathcal{F}([\rho_c^{(0)}(\mathbf{r}, \{R_i\}, \{\Omega_i\})], \{R_i\}, \{\Omega_i\})$$

$$= -\Omega_j \times \int d\mathbf{r}\rho_c^{(0)}(\mathbf{r}, \{R_i\}, \{\Omega_i\})\nabla_{\Omega_j} V_{mc}(\mathbf{r} - R_j, \Omega_j) \tag{17}$$

for $1 \leq j \leq N_m$. In order to obtain the total force $\mathbf{F}_j = \mathbf{F}_j^c + \mathbf{F}_j^m$ and the total torque $\mathbf{M}_j = \mathbf{M}_j^c + \mathbf{M}_j^m$ acting on rod j one must add the direct inter-rod forces

$$\mathbf{F}_j^m = -\nabla_{R_j} \sum_{i,k=1;i<k}^{N_m} V_{mm}(R_i - R_k, \Omega_i, \Omega_k) \tag{18}$$

and torques

$$\mathbf{M}_j^m = -\Omega_j \times \nabla_{\Omega_j} \sum_{i,k=1;i<k}^{N_m} V_{mm}(R_i - R_k, \Omega_i, \Omega_k). \tag{19}$$

Regarding Eqs. (16) and (17), one clearly sees the many-body character of the counterion-induced forces and torques: Only if the equilibrium density $\rho_c^{(0)}(\mathbf{r}, \{R_i\}, \{\Omega_i\})$ is a linear superposition of density orbitals around each rod, are the forces and torques pairwise. In general, however, the density will explicitly depend on the rod configuration and will be a complicated *nonlinear* combination of such density orbitals. This nonlinear counterion screening immediately results in effective many-body interactions between the rods.

At this stage it is useful to compare the present approach to other familiar approaches, namely the Poisson–Boltzmann approach and the linearized Debye–Hückel theory which are both special cases of the present theory. The Poisson–Boltzmann approach, recently used in an *ab initio* simulation by Fushiki[43] for spherical particles is obtained if the correlational part of counterionic free energy functional, $\mathscr{F}_{corr}$, is neglected completely. The Debye–Hückel theory is a further approximation if the local nonlinear ideal part $\mathscr{F}_{id}$ is expanded in the density difference $\rho_c(\mathbf{r}) - \rho_c$ around the mean counterion density ρ_c, see Ref. 36.

Now the general strategy of *ab initio* simulations is as follows. One starts with a given configuration $\{\mathbf{R}_i\}$, $\{\mathbf{\Omega}_i\}$ of rods in a periodically repeated simulational box. One then minimizes the free energy functional $\mathscr{F}$ with respect to the counterion density field and thus gains the total forces and torques on the rods. Then, using molecular dynamics described by the Lagrangian $\mathscr{L}$, the rods are moved with a small time step, $\mathscr{F}$ is again minimized, the forces and torques are again calculated, and the rods are moved again. After a sufficient number of equilibration time steps, statistics is taken during a big number of time steps and thus orientational and other pair correlations of the rods are calculated. It is clear that this strategy still requires an enormous numerical effort. We can avoid the major difficulties by adopting a pseudopotential construction and using the Car-Parrinello simulational method. This is described in detail in Sec. IV.

III. EFFECTIVE YUKAWA-SEGMENT MODELS

In this section we summarize effective segment models with Yukawa pair interaction between each segment along the rod. The DLVO-segment model is well known and was frequently used in theory and computer simulation whereas the second model, resulting from an optimal fit of the *ab initio* data, and an analytical Poisson–Boltzmann cell model are novel results of this paper. In an effective Yukawa-segment model the interaction energy between two rods is taken as the sum over screened Coulomb potentials between N_s segments on each of the rods:

$$V(\mathbf{r},\mathbf{\Omega}_1,\mathbf{\Omega}_2) = \sum_{\alpha,\beta=1}^{N_s} V_{\alpha\beta}^p \Bigg(\bigg\| \mathbf{r} + \mathbf{\Omega}_1 \frac{L}{2N_s} (2\alpha - 1 - N_s) \\ + \mathbf{\Omega}_2 \frac{L}{2N_s} (2\beta - 1 - N_s) \bigg\| \Bigg), \tag{20}$$

where $\mathbf{r}$ is the separation between the centers of mass of the rods, and $V_{\alpha\beta}^p(r)$ is a charge-polydisperse Yukawa potential

$$V_{\alpha\beta}^p(r) = \frac{Z_\alpha Z_\beta}{N_s^2} \frac{e^2}{\epsilon r} \exp(-\kappa r). \tag{21}$$

It is the explicit form of Z_α and κ which is the output of an effective Yukawa model.

A. DLVO-segment model

The simplest segment model is based on the traditional DLVO interaction between spherical particles[44,45] and was introduced and studied by Klein and co-workers.[29–31] In this model,

$$Z_\alpha = Z \exp(\kappa_{DH}R)/(1 + \kappa_{DH}R) \tag{22}$$

and

$$\kappa = \kappa_{DH} = \sqrt{\frac{4\pi e^2 q^2 Z \rho_m}{\epsilon k_B T}}. \tag{23}$$

It was shown by Dhont and Klein[32] that this DLVO segment model becomes exact at infinite dilution. For strong interactions or dense systems, however, there is no theoretical justification for the DLVO-segment model.

B. Optimal effective segment model by fitting the *ab initio* data

For this method, one needs to perform an *ab initio* run first. During the run one stores $\mathscr{N}_c$ different typical configurations $\{\mathbf{R}_i^{(j)}, \mathbf{\Omega}_i^{(j)}; i=1,...,N_m; j=1,...,\mathscr{N}_c\}$ and the associated many-body forces on the center of mass and the many-body torques $\{\mathbf{F}_i^{(j)}, \mathbf{M}_i^{(j)}; i=1,...,N_m; j=1,...,\mathscr{N}_c\}$. One then makes a least square fit with a segment model of pair potentials, i.e., one minimizes the forces

$$\sum_{j=1}^{\mathscr{N}_c} \sum_{i=1}^{N_m} \left(\mathbf{F}_i^{(j)} - \sum_{k=1;k\neq i}^{N_m} \frac{\partial V(\mathbf{r},\mathbf{\Omega}_i^{(j)},\mathbf{\Omega}_k^{(j)})}{\partial \mathbf{r}} \bigg|_{\mathbf{r}=\mathbf{R}_i^{(j)}-\mathbf{R}_k^{(i)}} \right)^2 \tag{24}$$

or the torques

$$\sum_{j=1}^{\mathscr{N}_c} \sum_{i=1}^{N_m} \left(\mathbf{M}_i^{(j)} - \sum_{k=1;k\neq i}^{N_m} \mathbf{\Omega}_i^{(j)} \frac{\partial V(\mathbf{R}_i^{(j)}-\mathbf{R}_k^{(i)},\mathbf{\Omega}_i^{(j)},\mathbf{\Omega}_k^{(j)})}{\partial \mathbf{\Omega}_i^{(j)}} \right)^2, \tag{25}$$

where $V(r,\mathbf{\Omega}_1,\mathbf{\Omega}_2)$ has the segment form (20) with a pairpotential $V_{\alpha\beta}^p(r)$. It is with respect to $V_{\alpha\beta}^p(r)$ and also with respect to L that Eqs. (24) and (25) are minimized. In the k sum of Eqs. (24) and (25) also periodic images must be taken into account if $V_{\alpha\beta}^p(r)$ is long ranged. We tried different *Ansätze* for $V_{\alpha\beta}^p(r)$ and made the following observations.

(i) For the minimizing potential, it practically does not matter whether one fits the forces (24) or the torques (25). The results are very close.

(ii) The best fit was achieved with a charge-polydisperse Yukawa-segment model. Also a fit with a usual (charge-monodisperse) Yukawa potential was acceptable. However, a fit where $V_{\alpha\beta}^p(r)$ is chosen as a soft sphere potential $V_{\alpha\beta}^p(r) = Ar^{-\nu}$ where A and ν are fitting parameters is much worse than a two-parameter Yukawa ansatz $V_{\alpha\beta}^p(r) = A \exp(-\nu r)/r$.

(iii) The optimal *ab initio* fit reproduces the *ab initio* data for the forces and torques within a relative error of $\lesssim 2\%$.

(iv) As will be explicitly demonstrated in Sec. V, the *ab initio* fit model reproduces the pair correlations of the *ab initio* run quite well. However, for higher order correlations and more subtle quantities where many-body forces become important, the results with the *ab initio* fit become worse.

(v) The *ab initio* fit does not depend sensitively on the number N_m of rods used in the *ab initio* run. If one calculates pair correlations in an *ab initio* simulation one must carefully consider finite size effects and one typically needs at least ≈ 100 rods in the simulational box. It is much less computationally costly to simulate a smaller system with say ≈ 15 rods, fit an optimal effective segment model, and then do a simulation with a big system size of this segment model.

Summarizing the *ab initio* fit represents an optimal effective segment model with pair potentials and is thus superior to any of other explicit segment models. However, one needs to perform an *ab initio* simulation of a small-sized sample first. We finally mention that in Ref. 37 the same idea of an *ab initio* fit was discussed in the case of spherical colloidal particles where the Yukawa pair potential, frequently used for the interaction between charged colloidal spheres, was justified.

C. An exactly soluble Poisson–Boltzmann-cell model

Another way to obtain explicitly parameters for an effective Yukawa-segment description for the interaction between charged rods results from a calculation of the counterion density profile in a cylindrical Wigner–Seitz cell (WSC) around one rod. For an infinite long rod, this density profile $\rho_{PB}(r)$ is analytically known in the nonlinear Poisson–Boltzmann approximation (PBA),[46,6] characterized by Poisson's

$$\frac{d^2\phi(r)}{dr^2} + \frac{1}{r}\frac{d\phi(r)}{dr} - k_BT\kappa^2\rho_{PB}(r)/\rho_c = 0 \qquad (26)$$

and Boltzmann's

$$\rho_{PB}(r) = \rho_c \exp\left(-\frac{\phi(r)}{k_BT}\right) \qquad (27)$$

equations, r being the cylindrical distance. We then match this profile at the WSC boundary with that of a linearized Debye–Hückel screening solution, where the associated screening constant κ_l is determined by the counterion density at the WSC boundary. The effective charge is then obtained by integrating the Debye–Hückel counterionic profile inside the WSC. In this way, one ends up with a simple analytical Poisson–Boltzmann cell (PBC) model. This model is justified (i) for long rods. $L/D \gtrsim 4$, since an infinite rod is taken as a reference system, (ii) for strong interactions, since only the Wigner–Seitz cell boundary is considered, and (iii) for small volume fractions, since the effective boundary is assumed to be cylindrical. It is thus quite complementary to the DLVO-segment model which works for infinite dilution or weak interactions, respectively. The idea of such a cell model was first used by Alexander et al.[34] for colloidal spheres. In the spherical case, however, one does not end up with analytical expressions as the solution of the PBA is not known exactly in spherical symmetry.

We consider an infinite long rod with a charge line density $z = Z/L$ along the rod in a cylindrical WSC which has an outer radius of $R_0 = 1/\sqrt{\pi L \rho_m}$. A typical measure for the charge density along the rod is the ratio $\xi = l_B z$ of the Bjerrum length $l_B = e^2/\epsilon k_BT$ and the linear spacing of one el-

ementary charge along the rod. Depending on the value of the WSC boundary density, $\rho_{PB}(R_0)$, there are two different cases: (i) $\rho_{PB}(R_0) < \rho_c^*$ and (ii) $\rho_{PB}(R_0) \geqslant \rho_c^*$, with a threshold density

$$\rho_c^* \equiv 1/2\,\pi l_B R_0^2. \qquad (28)$$

In case (i), the density profile is given by

$$\rho_{PB}(r) = \rho_{PB}(R_0)\frac{4\beta^2}{\lambda r\,\cos[\beta\,\ln(r/R_m)]^2}\,. \qquad (29)$$

Here, the dimensionless constant $\beta > 0$ is determined as a solution of the algebraic equation

$$\frac{1}{\beta}\,\arctan\left(\frac{\xi-1}{\beta}\right) + \frac{1}{\beta}\,\arctan\frac{1}{\beta} - \ln(R_0/R) = 0. \qquad (30)$$

Furthermore, in Eq. (29), the constant R_m is given by

$$R_m = R\,\exp\left[\frac{1}{\beta}\,\arctan\left(\frac{\xi-1}{\beta}\right)\right] \qquad (31)$$

and the screening constant λ is defined as $\lambda = 2\sqrt{1+\beta^2}/R_0$. The WSC boundary density is given via

$$\rho_{PB}(R_0) = \rho_c^*(1+\beta^2). \qquad (32)$$

On the other hand, in case (ii) the density profile is

$$\rho_{PB}(r) = \rho_{PB}(R_0)\frac{4\beta'^2}{\lambda' r\,\sinh[\beta'\,\ln(r/R_m')]^2}\,, \qquad (33)$$

where now the constant β' is determined by

$$\frac{1}{\beta'}\,\text{arcoth}\left(\frac{\xi-1}{\beta'}\right) + \frac{1}{\beta'}\,\text{arcoth}\frac{1}{\beta'} + \ln(R_0/R) = 0 \qquad (34)$$

with $\text{arcoth}(x) \equiv \frac{1}{2}\ln[(x+1)/(x-1)]$. Correspondingly, in case (ii), the constant R_m' in Eq. (33) is given by

$$R_m' = R\,\exp\left[-\frac{1}{\beta'}\,\text{arcoth}\left(\frac{\xi-1}{\beta'}\right)\right] \qquad (35)$$

and $\lambda' = 2\sqrt{1-\beta'^2}/R_0$. Now, the WSC boundary density equals

$$\rho_{PB}(R_0) = \rho_c^*(1-\beta'^2). \qquad (36)$$

We now consider solutions $\rho_l(r)$ of the linearized (Debye–Hückel) version of the Poisson–Boltzmann equation in a cylindrical WSC

$$\left(\frac{d^2}{dr^2} + \frac{1}{r}\frac{d}{dr} - \kappa_l^2\right)\rho_l(r) = 0, \qquad (37)$$

where the screening parameter κ_l is determined in terms of the WSC boundary density

$$\kappa_l^2 = \frac{4\pi e^2 q^2}{\epsilon k_BT}\,\rho_{PB}(R_0). \qquad (38)$$

This is an essential assumption meaning that the effective screening is only established by the counterions near the WSC boundary. Equation (37) has the general solution

$$\rho_l(r) = AI_0(\kappa_l r) + BK_0(\kappa_l r), \qquad (39)$$

where A, B are integration constants and $I_n(x)$, $K_n(x)$ denote Bessel functions of imaginary argument of order n.[47] The
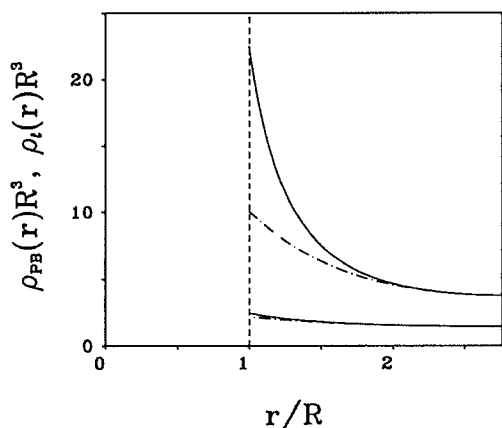
FIG. 1. Density profiles of the counterions in a cylindrical Wigner–Seitz cell for two different parameter combinations in units of $1/R^3$. The results of the linearized PBC model, $\rho_l(r)$ (dot-dashed lines), as well as that of the Poisson–Boltzmann theory, $\rho_{\mathrm{PB}}(r)R^3$ (solid lines), are shown. r denotes the cylindrical distance. The parameters are $R=53$ nm, $T=300$ K, $\epsilon=78$, $L/2R=6$, $\rho=6c^*$. For the lower curves, $Z=400$ and $\rho_{\mathrm{PB}}(R_0) < \rho_c^*$ whereas for the upper curves, $Z=1500$ and $\rho_{\mathrm{PB}}(R_0) > \rho_c^*$.

coefficients A and B are directly determined by matching the density at the WSC boundary with $\rho_{\mathrm{PB}}(R_0)$, i.e., by demanding $\rho_{\mathrm{PB}}(R_0)=\rho_l(R_0)$ and requiring $d\rho_l(R_0)/dr=0$ which is a direct consequence of global charge neutrality. Explicitly, one gets

$$B=\rho_{\mathrm{PB}}(R_0)\ \frac{I_1(\kappa_l R_0)}{I_1(\kappa_l R_0)K_0(\kappa_l R_0)+I_0(\kappa_l R)K_1(\kappa_l R)} \qquad (40)$$

and

$$A=B\ \frac{K_1(\kappa_l R_0)}{I_1(\kappa_l R_0)}. \qquad (41)$$

Finally, the effective charge Z_{PBC} of the rod is obtained by integrating the density profile[39]

$$Z_{\mathrm{PBC}}/L=2\pi\int_R^{R_0} dr\ r\rho_l(r)$$

$$=\frac{2\pi R}{\kappa_l}\ \rho_{\mathrm{PB}}(R_0)$$

$$\times\frac{I_1(\kappa_l R_0)K_1(\kappa_l R)-I_1(\kappa_l R)K_1(\kappa_l R_0)}{I_1(\kappa_l R_0)K_0(\kappa_l R_0)+I_0(\kappa_l R)K_1(\kappa_l R)}. \qquad (42)$$

In Fig. 1, the density profiles $\rho_{\mathrm{PB}}(r)$ and $\rho_l(r)$ are compared for two parameter combinations corresponding to cases (i) and (ii). The qualitative results are very similar to the spherical case.[34] First, the effective charge Z_{PBC}, is in general smaller than the bare charge Z and the corresponding screening length κ_l is smaller, too, compared to its Debye–Hückel value. Second, for very high Z, Z_{eff} is drastically reduced, and does only depend very weakly on Z. This is illustrated in Fig. 2. Nevertheless, since also κ_l decreases with increasing Z, the interaction may become stronger even than that of the DLVO-segment model. However, we emphasize that in the cylindrical symmetry the PBA is exactly soluble whereas

there is no such explicit solution in the spherical case and thus this model is more easily implemented in the cylindrical case.

The resulting PBC-Yukawa-segment model for the interaction between charged rods is finally given by

$$Z_\alpha=Z_{\mathrm{PBC}}, \quad \kappa=\kappa_l. \qquad (43)$$

IV. AB INITIO APPROACH: PRACTICAL IMPLEMENTATION

A. Pseudopotential construction

First of all, we have to fix the charge distribution $en_m(\mathbf{r},\Omega)$ of a rod with orientation Ω, whose center of mass is at the origin. One may expect that details of this distribution do not matter as long as typical spacings of the charge inhomogeneities are small compared to the mean distance between the rods. As in Refs. 35 and 36 we are using a classical pseudopotential construction in order to smooth the counterionic density profile at the macroionic surfaces. This is technically necessary and reduces the numerical effort drastically.

The pseudopotential construction is done as follows. We first put N_r equal charges $Z^{(0)}/N_r$ on equally spaced segments along the rod. Hence we start from a rod charge distribution

$$en_m^{(0)}(\mathbf{r},\Omega)=e\ \frac{Z^{(0)}}{N_r}\ \sum_{\alpha=1}^{N_r}\ \delta\left(\mathbf{r}-\Omega\ \frac{L^{(0)}}{2N_r}\ (2\alpha-1-N_r)\right), \qquad (44)$$

where $L^{(0)}$ is an a priori rod length. This is not the final real charge distribution $en_m(\mathbf{r},\Omega)$ since the pseudopotential construction admits penetrating counterions which will reduce the rod charge from $Z^{(0)}$ to Z. Also the final rod length will be slightly changed from $L^{(0)}$ to L.

In a second step, the rod-counterion potential $V_{mc}(\mathbf{r},\Omega)$ of Eq. (4) is replaced by the penetrable potential

$$V'_{mc}(\mathbf{r},\Omega)=-qe^2\int d\mathbf{r}'\ \frac{n_m^{(0)}(\mathbf{r}',\Omega)}{\epsilon}\ \mathrm{erf}\left(\frac{|\mathbf{r}-\mathbf{r}'|}{R_c}\right). \qquad (45)$$
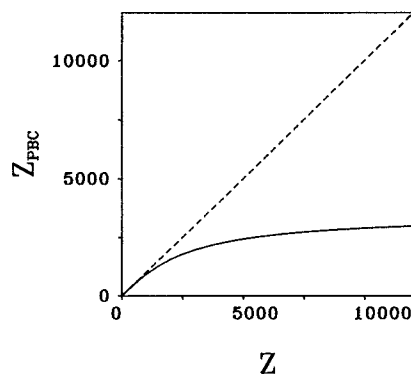

FIG. 2. Effective charge in the PBC model, Z_{PBC}, vs bare charge Z (solid line). The other parameters are as in Fig. 1. For comparison the straight line $Z_{\mathrm{PBC}}=Z$ is also shown (dashed line).
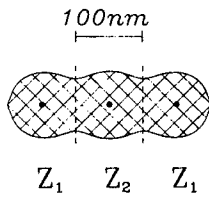
$100nm$

Z_1 Z_2 Z_1

FIG. 3. Cylindrical rod shape for the parameters corresponding to run A where $N_r=3$ and the three equal original point charges have a distance of 100 nm. The positions of these point charges are shown by the full black circles. Integration of the inside counterion density, which penetrates the core due to the pseudopotential construction, yields reduced values Z_1, Z_2 for the bare charges. In general $Z_1 \neq Z_2$. The integration boundaries are indicated by dashed lines.

Here $\text{erf}(x)$ denotes the error function and $R_c=2R$ is chosen in order to ensure that $V'_{mc}(\mathbf{r},\Omega)$ practically equals $V_{mc}(\mathbf{r},\Omega)$ outside the rod volume. As a consequence, the counterions will penetrate into the core.

In a third step, fluctuations of the inside counterions are suppressed by adding an arbitrary free energy penalty $f_{\text{cut}}(\rho_c)$ to $\Psi^{\text{exc}}_{\text{OCP}}(T,\rho_c)$ in Eq. (13) which increases rapidly for counterion densities $\rho_c > \rho_c^{\text{cut}}$; the form chosen for f_{cut} is

$$f_{\text{cut}}(\rho_c) = \begin{cases} 0 & \text{when } x \equiv (\rho_c - \rho_c^{\text{cut}})/\rho_c^{\text{cut}} < 0 \\ 0.05 \, \exp\left(-\dfrac{3}{\tan(\pi x)}\right) & \text{when } x \geq 0 \end{cases} \quad (46)$$

Here, ρ_c^{cut} is determined self-consistently as to match the averaged density at the rod surface having a cylindrical distance R from the origin. This cutoff density discriminates between two regions: For $\rho_c(\mathbf{r}) < \rho_c^{\text{cut}}$, fluctuations of the charge density are not affected by the free energy penalty, whereas for $\rho_c(\mathbf{r}) > \rho_c^{\text{cut}}$ the charge distribution is stiffened by the penalty. Consequently the form of the rod [or, in other terms, the boundary of the characteristic function $\chi(\mathbf{r},\Omega)$] is given by the two-dimensional manifold defined as the solution of

$$\rho_c(\mathbf{r}) = \rho_c^{\text{cut}}. \quad (47)$$

If one averages over different rods and different orientations during a simulation, the averaged value finally determines the actual form of the rods. It should be noted, however, that, due to the construction, the fluctuations in the rod shape are very small (less than 3%) and the resulting rod shape is very close to a spherocylinder. Obviously it depends on the linear charge spacing $L^{(0)}/N_r$ of the original charge distribution $en_m^{(0)}(\mathbf{r},\Omega)$. One possible rod shape for the parameters used in the simulation is shown in Fig. 3 where $N_r=3$. Having determined the rod shape, the rod volume $\mathcal{V}_m$ is readily obtained by integration.

By the free energy penalty (46), the fluctuations of the artificial counterion density inside the rod are suppressed. This was explicitly checked a posteriori in the simulation. The averaged counterion inside density $en_c^{(i)}(\mathbf{r},\Omega)$ has therefore to be added to the total charge distribution such that

$$n_m(\mathbf{r},\Omega) = n_m^{(0)}(\mathbf{r},\Omega) + n_c^{(i)}(\mathbf{r},\Omega). \quad (48)$$

Correspondingly, the total rod charge is reduced to a value Z being smaller than $Z^{(0)}$ as obtained by integrating $n_c^{(i)}(\mathbf{r},\Omega)$ over the rod volume.

One disadvantage compared to the case of spherical macroions[35,36] is that one cannot predict Z within one single run. One has to guess a suitable $n_m^{(0)}(\mathbf{r},\Omega)$ and determine ρ_c^{cut} and then one gets the total rod charge Z as an output. This means that one needs a set of iterative runs in order to get finally the prescribed result for Z. In the spherical case this could be done in a spherical Wigner–Seitz cell without any notable numerical effort since the radial coordinate was only relevant. In the case of cylindrical rods of finite length, however, this calculation is not trivial. In the following we just take some parameter combinations where Z is an output of an arbitrary chosen initial charge distribution $en_m^{(0)}(\mathbf{r},\Omega)$.

B. Car–Parrinello method

Following general ideas of Car and Parrinello[38] which were implemented in the classical context in Ref. 36 we add a small fake kinetic energy term

$$K_f = \frac{1}{2} \, m_f \int d\mathbf{r} [\dot\rho_c(\mathbf{r})]^2 \quad (49)$$

to the Lagrangian $\mathscr{L}$ from Eq. (7) with a small fake mass m_f. m_f was chosen such that the resulting counterionic fake kinetic energy during the run was less than 4% of the kinetic energy of the rods, thus ensuring that we are very close to the adiabatic solution.

We parametrize the counterion density field by its expansion in Fourier components

$$\rho_c(\mathbf{r}) = \sum_{\mathbf{k}} \rho_{\mathbf{k}c} \exp(i\mathbf{k}\cdot\mathbf{r}), \quad (50)$$

where the sum is over all reciprocal lattice vectors $\mathbf{k}$ of the periodically repeated simulation box of volume V. In practice, we include about $\mathscr{N}=850\,000$ different reciprocal lattice vectors and cut off the sum in Eq. (50). The resulting density in $\mathbf{r}$ space is defined on an $\mathscr{N}$-dimensional grid of the cubic or rectangular simulational box.

The finite difference versions of the equations of motion corresponding to the Lagrangian $\mathscr{L}+K_f$ are solved iteratively with a finite time-step Δt. Standard molecular dynamics algorithms for the orientational degrees of freedom of the rigid rods[48] are used. The center-of-mass motions are coupled to a Nosé thermostat,[49] such that averages taken along the phase space trajectories are equivalent to canonical ensemble averages at an imposed temperature T. The angular velocities were scaled each 200 steps to this prescribed temperature. Efficient fast Fourier transform techniques are used to commute back and forth between the $\mathbf{r}$- and $\mathbf{k}$-space representations of the counterion density. The infinite range of the bare Coulomb interactions is taken care of by appropriate Ewald summation.[48] The finite time-step Δt was chosen sufficiently small to ensure excellent conservation of the total energy of the system.

TABLE I. Parameters and results of the *ab initio* run A (AI) and the different Yukawa-segment models: the *ab initio* fit (AI fit), the DLVO, and the PBC model. Given are the outer charge Z_1 and the inner charge Z_2 along the rod (see Fig. 3), the distance d between these charges, the inverse screening length κ in the different Yukawa-segment models, the mean force $\bar{F}$, and the mean torque $\bar{M}$. For the *ab initio* run, Z_1 and Z_2 are just the total integrated inside charge of Fig. 3 with distance d. Z_1, Z_2, d, and κ were used as four independent fit parameters to find an optimal *ab initio* fit potential within a three-segment model. For the DLVO and PBC model the charges are assumed to be equal and the quadrupole moment of the original charge distribution is matched in finding a suitable d for a three-segment model.

Model	Z_1	Z_2	d(nm)	κR	$\bar{F}/k_B T \rho_m^{1/3}$	$\bar{M}/k_B T$
AI	46.4	43.8	100.7	-	29.8	9.3
AI fit	66.5	66.4	100.8	0.6471	29.0	9.0
DLVO	51.4	51.4	101.7	0.5752	23.7	7.4
PBC	45.3	45.3	101.7	0.6462	18.7	5.9

V. RESULTS

Three different *ab initio* runs were performed in the disordered fluid as well as in the liquid crystalline (smectic B) phase. The results are compared with that of Yukawa-segment models. In every run the temperature was fixed to $T=300$ K (room temperature) and the dielectric constant is that of water, $\epsilon=78$.

A. Disordered phase

One parameter combination (run A) was in the fluid phase. $N_m=108$ rods were put into a periodically repeated cubic simulational box with $\mathscr{N}=96^3$ gridpoints. The original charge distribution $en_m^{(0)}(\mathbf{r},\mathbf{\Omega})$ was taken according to Eq. (44) with $N_r=3$, $Z^{(0)}/N_r=65$, $L^{(0)}=302$ nm. The pseudopotential construction then yields the bare charges $Z_1=46.4$ and $Z_2=43.8$ (see Fig. 3) such that the total rod charge is $Z=2Z_1+Z_2=136.6$. The rod shape has an averaged cylindrical radius of $R=47$ nm and a total length of $L=301$ nm, hence $L/2R=3.2$. The cutoff density ρ_c^{cut} was $2.77/R^3$. The rod density was $\rho_m=3.34c^*=3.34/L^3$ which corresponds to a concentrated system with a relatively high volume fraction $\phi=0.23$. A very short-ranged steep repulsive potential was added in order to prevent overlapping rods. Nonetheless such overlapping was found to be rather unlikely. The moment of inertia, Θ, was chosen to be $\Theta=20MR^2$, M being the total mass which sets the time scale. The finite time step was $\Delta t=3\times10^{-3}\tau_0$ where $\tau_0=\sqrt{MR^2/k_B T}$. The starting positions were equilibrated positions gained by a run based on the DLVO-segment model. After an equilibration period of 8000 time steps, statistics were gathered over 25 000 time steps. One time step took about 4 s CPU time on a Cray YMP.

In Table I, the parameters of the three different Yukawa-segment models are given. Three segments are chosen and the distance between the point charges is fixed by matching the quadrupolar moment of the *ab initio* and the segment charge distribution. In the *ab initio* fit, this distance as well as the three point charges and the inverse screening length κ were taken as variational parameters and determined by minimizing Eq. (24) or Eq. (25). Due to the high volume fraction of the system the inverse screening length κ is higher in the PBC model than in the DLVO model and closer to that of the *ab initio* fit. The effective charges, however, are

both significantly lower than that resulting from the optimal Yukawa-segment model.

Two self-properties and some central pair correlations were calculated. First the mean force on the center of mass of the rods is defined as

$$\bar{F}=\frac{1}{N_m}\sum_{j=1}^{N_m}\sqrt{\langle\mathbf{F}_j^2\rangle},\tag{51}$$

where $\langle\cdots\rangle$ denotes a canonical average. In analogy the mean torque is

$$\bar{M}=\frac{1}{N_m}\sum_{j=1}^{N_m}\sqrt{\langle\mathbf{M}_j^2\rangle}.\tag{52}$$

Data for $\bar{F}$ and $\bar{M}$ are given in Table I for the *ab initio* run and the Yukawa models. For the Yukawa-segment model we took the same system size with $N_m=108$ particles in order to avoid systematic deviations due to finite system size in a comparison. Whereas both the PBC model and the DLVO model underestimate the mean forces and torques, the *ab initio* fit reproduces the *ab initio* data reasonably well.

As for pair correlations we have computed the pair correlation function of the center of mass

$$g(r)=\frac{1}{\rho_m N_m}\sum_{i,j=1;i\neq j}^{N_m}\langle\delta[\mathbf{r}-(\mathbf{R}_i-\mathbf{R}_j)]\rangle.\tag{53}$$

Orientational pair correlations are conveniently measured by the function[1]

$$g_P(r)=\frac{1}{\rho_m N_m g(r)}\sum_{i,j=1;i\neq j}^{N_m}\langle P_2(\cos\theta_{ij})\delta[\mathbf{r}-(\mathbf{R}_i-\mathbf{R}_j)]\rangle,\tag{54}$$

where θ_{ij} is the angle between two orientations $\mathbf{\Omega}_i$ and $\mathbf{\Omega}_j$ and $P_2(x)=(3x^2-1)/2$ is the second Legendre polynomial. If $g_P(r)$ is positive, two rods at a given center-of-mass distance r are on average oriented in parallel whereas they are perpendicular if $g_P(r)$ has a negative sign. For Yukawa-segment models it is known[1] that $g_P(r)$ is negative for small distances, becomes positive with a maximum roughly at mean distance $a=\rho_m^{-1/3}$, and finally tends oscillatory to zero as $r\to\infty$.

Finally the r-dependent force and torque pair correlations are defined via

$$g_F(r) = -\frac{1}{\rho_m N_m g(r)(k_B T \rho_m^{1/3})^2}$$

$$\times \sum_{i,j=1;i\neq j}^{N_m} \langle \mathbf{F}_i \cdot \mathbf{F}_j \delta[\mathbf{r}-(\mathbf{R}_i-\mathbf{R}_j)]\rangle, \tag{55}$$

and

$$g_M(r) = -\frac{1}{\rho_m N_m g(r)(k_B T)^2}$$

$$\times \sum_{i,j=1;i\neq j}^{N_m} \langle \mathbf{M}_i \cdot \mathbf{M}_j \delta[\mathbf{r}-(\mathbf{R}_i-\mathbf{R}_j)]\rangle. \tag{56}$$

The functions $g_F(r)$ and $g_M(r)$ diverge to $+\infty$ as $r\to 0$ and vanish in the opposite limit $r\to\infty$.

Results for the pair correlations are shown in Fig. 4 both for the *ab initio* run and the Yukawa models. The pair correlation function $g(r)$ which is displayed in Fig. 4(a) does not exhibit a great structure since the system is disordered and

correlations of the center-of-mass coordinates are mainly smeared out by a large number of different rod configurations. Figure 4(b) shows orientational correlations as embodied in $g_P(r)$. The DLVO and the PBC segment model underestimate the structure whereas there is quite good agreement between the *ab initio* data and the *ab initio* fit within the statistical error. The discrepancies are readily explained with many-body interactions between the rods which are ignored in the *ab initio* fit procedure. Finally the force and torque correlation functions are shown in Figs. 4(a) and 4(b). Although there is a considerable statistical error, one can conclude that the correlations are reasonably reproduced by the *ab initio* fit, not too surprisingly, since the forces and torques were adjusted in this theory, while again both DLVO and PBC model underestimate the forces and torques. $g_M(r)$ shows an oscillation near the averaged distance $a = \rho_m^{-1/3}$.

The underestimation of the structure by the DLVO and PBC model can also be seen more directly if one takes the Yukawa-segment data of Fig. 1 and plots the force between two infinitely long parallel rods carrying a line charge density $z = Z/L$ which are separated by a distance r. In a liquid-crystalline situation where neighboring rods are really paral-
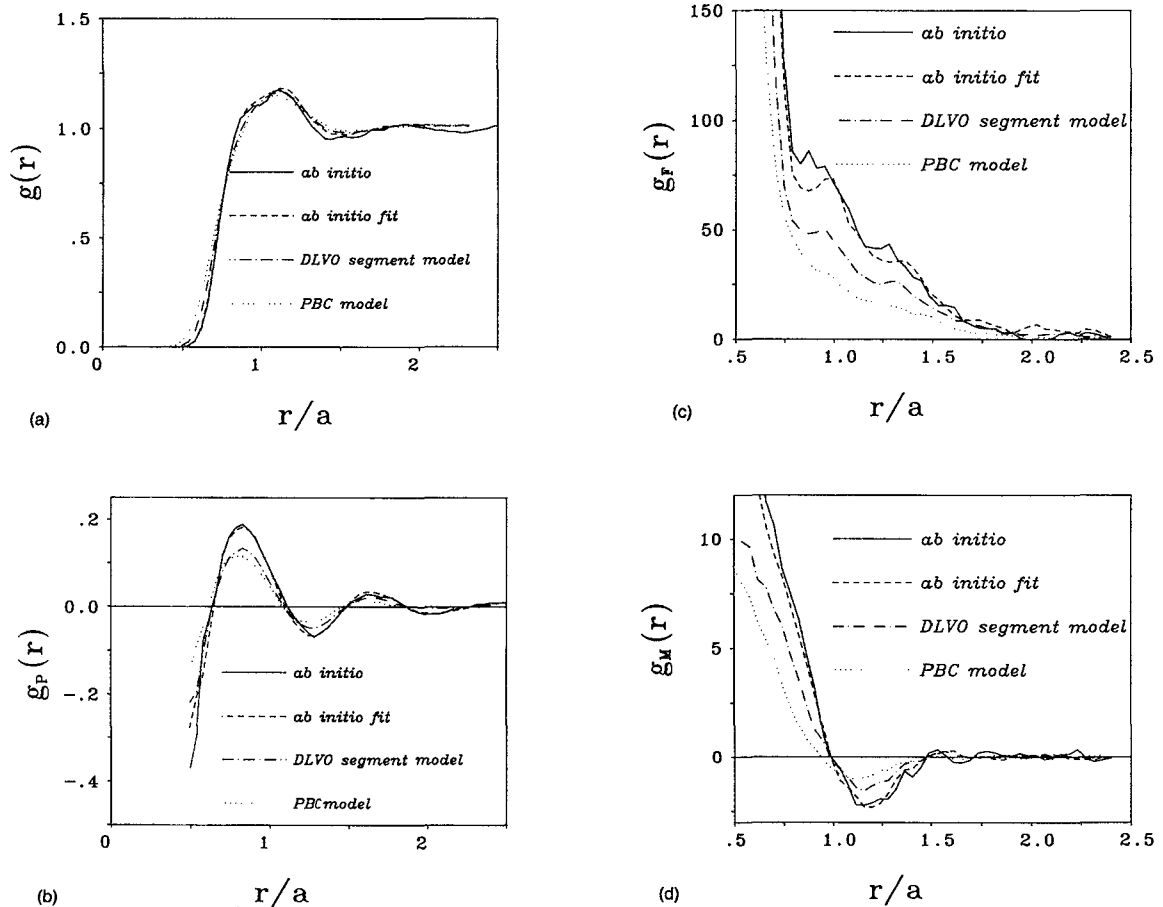

(a)

(b)

(c)

(d)

FIG. 4. Different pair correlation functions as a function of the center-of-mass distance r measured in terms of the mean distance $a = \rho_m^{-1/3}$. (a) Pair correlation function $g(r)$ of the center-of-mass coordinate. (b) Orientational correlation function $g_P(r)$ as defined in the text. (c) Force correlation function $g_F(r)$ as defined in the text. (d) Torque correlation function $g_M(r)$ as defined in the text. For the parameters of run A results are shown for the *ab initio* calculation (solid lines), the Yukawa-segment model by *ab initio* fit (dashed lines), the DLVO-segment model (dot-dashed lines), and the PBC-segment model (dotted lines).
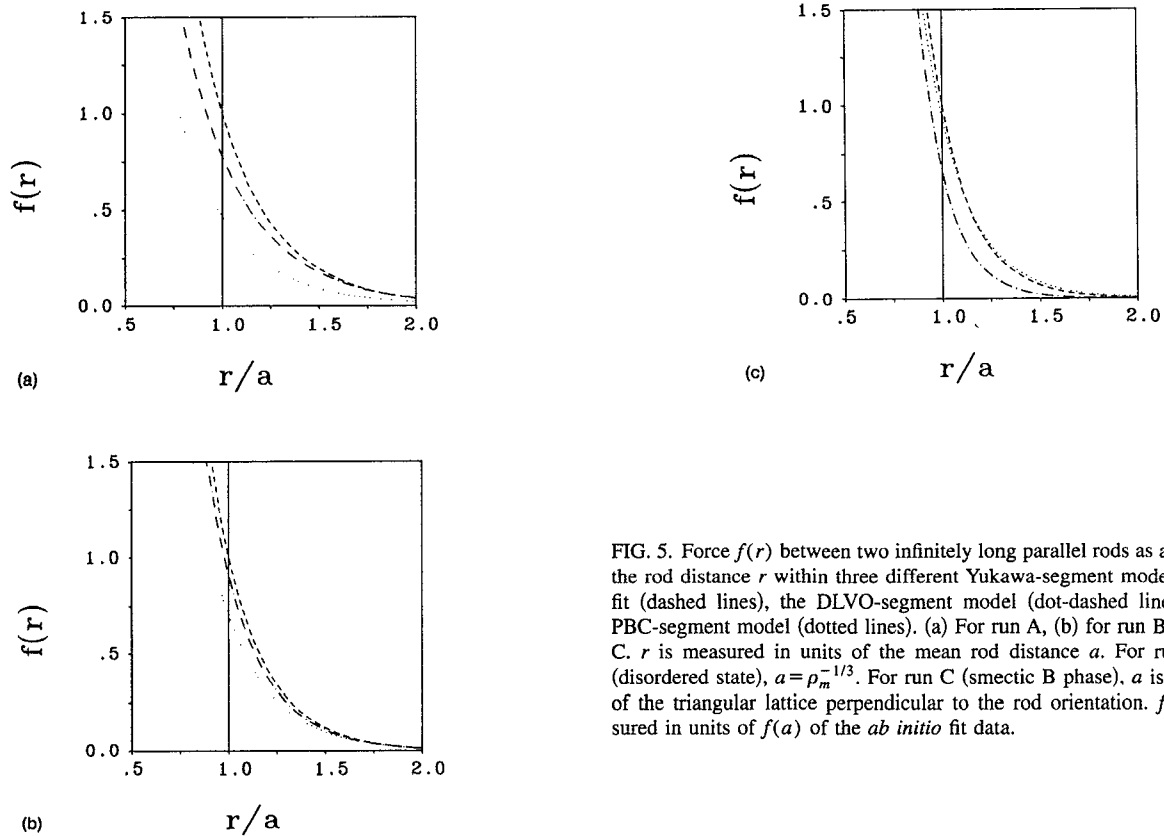
(a) r/a

(c) r/a

(b) r/a

FIG. 5. Force $f(r)$ between two infinitely long parallel rods as a function of the rod distance r within three different Yukawa-segment models: *ab initio* fit (dashed lines), the DLVO-segment model (dot-dashed lines), and the PBC-segment model (dotted lines). (a) For run A, (b) for run B, (c) for run C. r is measured in units of the mean rod distance a. For run A and B (disordered state), $a = \rho_m^{-1/3}$. For run C (smectic B phase), a is the spacing of the triangular lattice perpendicular to the rod orientation. $f(r)$ is measured in units of $f(a)$ of the *ab initio* fit data.

lel these forces are even very close to the actual forces. In a disordered configuration considered here these forces give only a qualitative estimate of the actual forces. The potential $v(r) = V(r)/L$ per unit length between two infinitely long rods of a Yukawa-segment model with inverse screening length κ is given by[50]

$$v(r) = \frac{(ze)^2}{\epsilon} K_0(\kappa r) \tag{57}$$

such that the forces are proportional to

$$f(r) = -\frac{dv}{dr} = \frac{(ze)^2}{\epsilon} \kappa K_1(\kappa r) \tag{58}$$

with K_0 and K_1 denoting Bessel functions of imaginary argument. This quantity is shown for the three different Yukawa-segment models in Fig. 5(a). Mainly the contribution from the mean distance is relevant if one relates $f(r)$, e.g., to the first peak of $g_P(r)$. As already expected from the results of the pair correlation functions, the DLVO and the PBC models underestimate the data of the *ab initio* fit. In the following we shall study the quantity $f(r)$ instead of a full simulation of the pair correlations. It gives already the right tendency of whether a Yukawa-segment model over- or underestimates the structure.

The failure of the DLVO model in run A is similar to the underestimation of the structure in spherical macroions for large packing fractions.[35,36] On the other hand, the PBC model fails for three reasons. First, the rods are not long enough to justify an *infinite* cylindrical symmetry. Second,

there are important configurations where the rods are perpendicular which cannot be described within a *cylindrical* Wigner–Seitz cell. Third, due to the high packing fraction the rods come close to each other and the approximation made in PBC theory that only the Wigner–Seitz *boundary* is relevant breaks down as well. The fact that the *ab initio* fit gives reasonable agreement with the full *ab initio* data enables us to calculate the pair correlations even for longer rods where one needs a large system in order to prevent finite size effects. The procedure then is to do a full *ab initio* run for a small system, to find an optimal Yukawa-segment model by fitting the forces and to then perform a simulation with the Yukawa-segment model for a large system.

We have followed this strategy for a second run, B, where a higher rod charge $Z = 442.8$ and a lower volume fraction $\phi = 0.10$ was chosen. The further parameters are given in the caption of Table II, where the results of the three Yukawa-segment models are shown. The force $f(r)$ of run B

TABLE II. *Ab initio* fit (AI fit), the DLVO, and the PBC model corresponding to run B. The meaning of the symbols is as in Table I. The parameters of run B are $N_m = 53$, $\mathcal{N} = 96^3$, $N_r = 3$, $L^{(0)} = 302$ nm, $Z_1 = 152.4$, $Z_2 = 138.0$, $R = 53$ nm, $L = 301$ nm, $\rho_c^{cut} = 6.2/R^3$, and $\rho_m = 1.31 c^*$.

Model	Z_1	Z_2	d(nm)	κR
AI fit	187.0	187.7	101.3	0.7347
DLVO	177.2	177.2	102.3	0.7328
PBC	136.0	136.0	102.3	0.6734

TABLE III. *Ab initio* fit (AI fit), the DLVO, and the PBC model corresponding to run C. Given are the line charge density z and the screening parameter κ, the Lindemann parameter L_{xy} of the triangular lattice in a smectic layer, orientational fluctuations χ_Ω as well as the mean force $\bar{F}$ and the mean torque $\bar{M}$.

Model	zR	κR	L_{xy}	$\chi_\Omega \times 10^4$	$\bar{F}/k_B T \rho_m^{1/3}$	$\bar{M}/k_B T$
AI fit	106.8	0.7329	0.06	4.0	198	199
DLVO	164.0	0.9417	0.09	6.5	189	190
PBC	81.8	0.6559	0.06	4.3	197	198

is shown in Fig. 5(b). For this moderate packing fraction, the DLVO model is a better description of the *ab initio* fit data than for run A. This agreement is, however, fortuitous as observed for spherical macroions[35,36] with similar parameters. Again the PBC model which is not expected to work in the fluid phase does underestimate the forces considerably.

B. Liquid-crystalline phase

We have performed a third run C in the liquid-crystalline (smectic B) phase. $N_m = 9$ rods were put into a periodically repeated rectangular box which is quadratic in x and y direction with $\mathcal{N} = 96 \times 96 \times 192$ gridpoints. The mean orientation of the rods was along the z direction. Due to resolution problems of the counterionic density field, only one smectic layer of rods could be simulated. In order to avoid a spurious center-of-mass diffusion in z direction, the z coordinate of the center of mass of the rods was fixed.

The original charge distribution $en_m^{(0)}(\mathbf{r},\Omega)$ was taken according to Eq. (44) with $N_r = 52$, $Z^{(0)}/N_r = 180$, $L^{(0)} = 1590$ nm. The pseudopotential construction yields a total line charge density of $z = Z/L = 2.89$ nm^{-1} along the rod and a cutoff density of $\rho_c^{cut} = 24./R^3$ where $R = 37.1$ nm is the averaged rod radius and $L = 1664$ nm is the total rod length such that $L/2R = 22.4$. The rod density is $\rho_m = 45.80c^*$ which corresponds to a packing fraction of $\phi = 0.070$. In the smectic layer the area density of the rods is $0.026/R^2$.

Sufficient configurations were gathered during an *ab initio* run of this small system and an optimal effective Yukawa-segment model was fitted to these configurations. The results together with that of the DLVO- and PBC-segment models are given in Table III. The PBC screening constant κ is much closer to the *ab initio* fit value than that of the DLVO model. The effective charge is a bit lower but the force is very much equal since the screening constant is a bit smaller. If one considers the forces $f(r)$ of these three models in Fig. 5(c), it becomes evident that the PBC model practically yields the same forces as the *ab initio* fit and is superior to the DLVO model. Note that the forces $f(r)$ are now physical since we are discussing an aligned liquid crystalline phase where the main interaction is that between parallel rods.

In order to check whether the PBC and the *ab initio* model also yield agreement of more subtle quantities we have performed simulations with a much larger system size of $N_m = 144$ rods (4 layers with 36 rods each of which having 14 segments). As a target quantity we first calculated the Lindemann parameter L_{xy} of the triangular lattice in one smectic layer which is defined as

$$L_{xy} = \frac{\sqrt{\langle (x - \langle x \rangle)^2 + \langle (y - \langle y \rangle)^2 \rangle \rangle}}{a_\Delta}, \tag{59}$$

where a_Δ is the lattice constant of the triangular lattice and $\mathbf{R} = (x,y,z)$ is the center-of-mass position of one rod whose mean orientation is in z direction. Second, orientational fluctuations are defined via

$$\chi_\Omega = \langle \Omega^2 \rangle - \langle \Omega \rangle^2 = 1 - \langle \Omega \rangle^2. \tag{60}$$

The quantity χ_Ω equals 1 in a disordered phase and is zero in a fully aligned configuration. Finally we have also calculated the mean forces and torques. The results are listed up in Table III. Again the PBC data are very close to the *ab initio* fit data whereas the DLVO segment model underestimates the structure.

In conclusion, in a liquid crystalline phase for long rods, the PBC model yields excellent agreement with the *ab initio* data. This is easily understood since the PBC model was designed for infinitely long rods in a spherical geometry which is well realized in a liquid crystalline phase. One may expect that the PBC model should also work in the nematic phase where the rods are still oriented.

VI. CONCLUSIONS

Summarizing, an *ab initio* description of nonlinear counterion screening in charged rodlike colloidal suspensions was described and implemented. It represents a combination of molecular dynamics for the mesoscopic charged rods and classical density functional theory for the microscopic counterions. Within this approach counterion-induced effective many-body forces between the rods are included. By fitting the forces and torques in actual configurations during the *ab initio* simulation an optimal effective pair potential segment model was extracted which is very close to a Yukawa-segment model. Thus the Yukawa-segment model frequently used to describe the interaction between charged rods is justified on an *ab initio* basis. The actual parameters for the effective charge and the screening constant, however, differ in general from that of the usual DLVO-segment model. This was demonstrated using three different runs in the disordered and liquid-crystalline phase. For partially aligned long rods, an exactly soluble Poisson–Boltzmann model in a cylindrical Wigner–Seitz cell was proposed. This model makes reasonable predictions for the inter-rod forces and is superior to the DLVO model in smectic and nematic phases of highly interacting rods.

The simple Poisson–Boltzmann-cell model can be used in theory and simulation as an effective Yukawa-segment

model. Within this model even quantitative agreement between experimental data for, e.g., TMV and the simulations may be achieved in liquid-crystalline-like phases. Furthermore the PBC model is readily generalized to a situation with added salt. This generalization and also a comparison with experimental data will be part of our future activity.

A further extension is to address *dynamical* quantities like orientational and center-of-mass self-diffusion of interacting rods. The true dynamics of the rods is Brownian[51] rather than molecular dynamics. As explicitly demonstrated for spherical macroions the *ab initio* description can at least in principle be generalized to Brownian dynamics of the macroparticles. It would be interesting to compare then dynamical quantities of the simulation with the available experimental results.

ACKNOWLEDGMENT

[1] R. Klein, in *Structure and Dynamics of Strongly Interacting Colloids and Supramolecular Aggregates in Solution*, edited by S. H. Chen, J. S. Huang, and P. Tartaglia, NATO ASI (Kluwer, Academic, 1992), Vol. 369.

[2] H. N. W. Lekkerkerker, Physica A **176**, 1 (1991).

[3] H. N. W. Lekkerkerker, in Ref. 1.

[4] F. P. Booy and A. Fowler, Int. J. Biol. Macromol. **7**, 327 (1985).

[5] Y. Hendrikx, J. Charvolin, M. Raviso, L. Liébert, and M. C. Holmes, J. Phys. Chem. **87**, 3991 (1983).

[6] C. F. Wu, S. H. Chen, L. B. Shih, and J. S. Lin, Phys. Rev. Lett. **61**, 645 (1988).

[7] Y. Maeda and S. Hachisu, Colloid Surf. **6**, 1 (1983); **7**, 357 (1983).

[8] J. Bugosh, J. Phys. Chem. **65**, 1791 (1961).

[9] T. Folda, H. Hoffmann, H. Chanzy, and P. Smith, Nature (London) **333**, 55 (1988).

[10] M. Nagy and A. Keller, Polym. Commun. **30**, 133 (1989).

[11] F. C. Bawden, N. W. Pirie, J. D. Bernal, and I. Fankuchen, Nature **138**, 1051 (1936).

[12] R. Oldenbourg, X. Wen, R. B. Meyer, and D. L. D. Caspar, Phys. Rev. Lett. **61**, 1851 (1988).

[13] X. Wen, R. B. Meyer, and D. L. D. Caspar, Phys. Rev. Lett. **63**, 2760 (1989).

[14] S. Fraden, G. Maret, D. L. D. Caspar, and R. B. Meyer, Phys. Rev. Lett. **63**, 2068 (1989).

[15] S. F. Schulz, E. E. Maier, and R. Weber, J. Chem. Phys. **90**, 7 (1989).

[16] M. Hagenbüchle, B. Weyerich, M. Deggelmann, C. Graf, R. Krause, E. E. Maier, S. F. Schulz, R. Klein, and R. Weber, Physica A **169**, 29 (1990).

[17] S. F. Schulz, E. E. Maier, R. Krause, M. Hagenbüchle, M. Deggelmann, and R. Weber, J. Chem. Phys. **92**, 7087 (1990).

[18] C. Graf, M. Deggelmann, M. Hagenbüchle, H. Kramer, R. Krause, C. Martin, and R. Weber, J. Chem. Phys. **95**, 6284 (1991).

[19] M. Hagenbüchle, C. Graf, and R. Weber, Progr. Colloid Polym. Sci. **89**, 49 (1992).

[20] E. E. Maier, R. Krause, M. Deggelmann, M. Hagenbüchle, R. Weber, and S. Fraden, Macromolecules **25**, 1125 (1992).

[21] S. Fraden, A. J. Hurd, R. B. Meyer, M. Cahoon, and D. L. D. Caspar, J. Phys. Colloq. C **3**, 85 (1985).

[22] L. Onsager, Ann. N. Y. Acad. Sci. **51**, 627 (1949).

[23] A. Stroobants, H. N. W. Lekkerkerker, and T. Odijk, Macromolecules **19**, 2232 (1986).

[24] J. A. C. Veerman and D. Frenkel, Phys. Rev. A **41**, 3237 (1990).

[25] A. Poniewierski and R. Holyst, Phys. Rev. Lett. **61**, 2461 (1988).

[26] A. M. Somoza and P. Tarazona, Phys. Rev. Lett. **61**, 2566 (1988).

[27] A. Poniewierski and R. Holyst, Phys. Rev. A **41**, 6871 (1990).

[28] H. Xu, H. N. W. Lekkerkerker, and M. Baus, Europhys. Lett. **17**, 163 (1992).

[29] J. Schneider, W. Hess, and R. Klein, J. Phys. A. **18**, 1221 (1985).

[30] J. Schneider, W. Hess, and R. Klein, Macromolecules **19**, 1729 (1986).

[31] J. Schneider, D. Karrer, J. K. G. Dhont, and R. Klein, J. Chem. Phys. **87**, 3008 (1987).

[32] J. K. G. Dhont and R. Klein, Colloid Polymer Sci. **265**, 289 (1987).

[33] E. Canessa, B. D'Aguanno, B. Weyerich, and R. Klein, Mol. Phys. **73**, 175 (1991).

[34] S. Alexander, P. M. Chaikin, P. Grant, G. J. Morales, P. Pincus, and D. Hone, J. Chem. Phys. **80**, 5776 (1984).

[35] H. Löwen, P. A. Madden, and J. P. Hansen, Phys. Rev. Lett. **68**, 1081 (1992).

[36] H. Löwen, J. P. Hansen, and P. A. Madden, J. Chem. Phys. **98**, 3275 (1993).

[37] H. Löwen and G. Kramposthuber, Europhys. Lett. **23**, 673 (1993).

[38] R. Car and M. Parrinello, Phys. Rev. Lett. **55**, 2471 (1985).

[39] R. J. Bacquet and P. J. Rossky, J. Phys. Chem. **88**, 2660 (1984).

[40] C. S. Murthy, R. J. Bacquet, and P. J. Rossky, J. Phys. Chem. **89**, 701 (1985).

[41] J. K. G. Dhont, J. Chem. Phys. **85**, 5983 (1986).

[42] R. Abe, Progr. Theor. Phys. **22**, 213 (1959).

[43] M. Fushiki, J. Chem. Phys. **97**, 6700 (1992).

[44] B. V. Derjaguin and L. D. Landau, Acta Physicochim. USSR **14**, 633 (1941).

[45] E. J. W. Verwey and J. T. G. Overbeek, *Theory of the Stability of Lyophobic Colloids* (Elsevier, Amsterdam, 1948).

[46] T. Alfrey, P. W. Berg, and H. Morawetz, J. Polym. Sci. **7**, 543 (1951).

[47] I. S. Gradshteyn and I. M. Ryzhik, *Tables of Integrals, Series and Products* (Academic, New York, 1965).

[48] M. P. Allen and D. J. Tildesley, *Computer Simulation of Liquids* (Clarendon, Oxford, 1989).

[49] S. Nosé, Mol. Phys. **52**, 255 (1984).

[50] E. Chang and D. Hone, J. Phys. France **49**, 25 (1988).

[51] M. Doi and S. F. Edwards, *The Theory of Polymer Dynamics* (Oxford University Press, Oxford, 1986).